Check for updates

Geophysical Research Letters

RESEARCH LETTER
10.1029/2020GL092257

Key Points:

- Very low sound velocities in B2-FeSi, a candidate phase at the CMB, measured up to 115 GPa and 1600 K by NIS
- Negligible anharmonic contributions to sound velocities validate the extrapolation of Birch's law to CMB conditions
- Less than 8.4 vol% B2-FeSi produced by core-mantle reactions are enough to explain the seismic anomalies associated with the ULVZs

Supporting Information:

Supporting Information may be found in the online version of this article.

Correspondence to:

V. Mergner and I. Kupenko,
v.mergner@fz-juelich.de;
kupenko@uni-muenster.de

Citation:

Mergner, V., Kupenko, I., Spiekermann, G., Petitgirard, S., Libon, L., Chariton, S., et al. (2021). Sound velocities in FeSi at lower mantle conditions and the origin of ultralow-velocity zones. *Geophysical Research Letters*, *48*, e2020GL092257. https://doi.org/10.1029/2020GL092257

Received 6 JAN 2021
Accepted 24 JUN 2021

© 2021. The Authors.
This is an open access article under the terms of the Creative Commons Attribution-NonCommercial-NoDerivs License, which permits use and distribution in any medium, provided the original work is properly cited, the use is non-commercial and no modifications or adaptations are made.

Sound Velocities in FeSi at Lower Mantle Conditions and the Origin of Ultralow-Velocity Zones

V. Mergner[1], I. Kupenko[1], G. Spiekermann[2], S. Petitgirard[3], L. Libon[2], S. Chariton[4], M. Krug[1], R. Steinbrügge[5], I. Sergueev[5], and C. Sanchez-Valle[1]

[1]Institut für Mineralogie, Universität Münster, Münster, Germany, [2]Institut für Geowissenschaften, Universität Potsdam, Potsdam, Germany, [3]Institut für Geochemie und Petrologie, ETH Zürich, Zurich, Switzerland, [4]Bayerisches Geoinstitut (BGI), Bayreuth, Germany, [5]Deutsches Elektronen-Synchrotron DESY, Hamburg, Germany

Abstract The origin of ultralow-velocity zones (ULVZs) remains an open question despite recent advances in mineral physics and seismology. Here, we examine the hypothesis that FeSi formed from core-mantle chemical reactions is a plausible source of ULVZs at the core-mantle boundary (CMB). The sound velocities of B2-structured FeSi were measured up to 115(2) GPa and 1600(200) K by nuclear inelastic scattering (NIS) in laser-heated diamond anvil cells (LH-DACs). Within uncertainties, the sound velocities of B2-FeSi display negligible anharmonicity, hence validating the extrapolation of velocity-density relations (Birch's law) to *P*-*T* conditions of the CMB. The sound velocities of B2-FeSi are significantly lower compared to other candidate phases in a lowermost mantle assemblage, and the Preliminary Reference Earth Model at CMB conditions. Less than 8.4 vol% of FeSi in the aggregate is thus sufficient to explain both the velocity decrements and the high density anomaly observed in a wide range of ULVZs.

Plain Language Summary Seismic studies have revealed patches on the Earth's core-mantle boundary (CMB), which have extremely low seismic velocities. However, the origin of these so-called ultralow-velocity zones (ULVZs) remains unclear. One plausible source could be FeSi, which is assumed to form from chemical reactions between material from the core and the mantle. Here, we test this hypothesis in an experimental study, where the elastic behavior of FeSi is measured while the sample is exposed to very high pressures and temperatures comparable to those in the Earth's lower mantle. From these measurements we derived the sound velocities of the high-pressure phase of FeSi at the CMB. We found that the sound velocities of FeSi are significantly lower than those of the average lowermost mantle measured in seismic studies, and also lower than those of other mineral phases in this region, which are also considered as potential sources of ULVZs. FeSi is thus a plausible candidate to explain the origin of ULVZs. Our results show that less than 8.4% of FeSi by volume in the aggregate are enough to explain both the amplitude of the velocity reduction and the high density anomaly observed in a wide range of ULVZs.

1. Introduction

The lowermost 150–300 km thick layer of the mantle overlying the core-mantle boundary (CMB), the so-called D" layer, is a highly complex setting which displays strong lateral heterogeneity of properties, such as electrical conductivity, seismic wave velocity, and density (e.g., Hernlund & McNamara, 2015; Lay, 2015; Lay et al., 1998). One of the unique features revealed by seismic investigations are the ultralow-velocity zones (ULVZs), that is, small, localized patches of ~10 km thickness and with large lateral spread of several hundred kilometers width atop of the CMB (Garnero & Helmberger, 1996; Revenaugh & Meyer, 1997). These features exhibit strong negative velocity anomalies of up to 5%–20% for P-waves and 10%–30% for S-waves relative to PREM (Garnero & Helmberger, 1996; McNamara et al., 2010; Thorne & Garnero, 2004) while the density typically increases by 5% (Reasoner & Revenaugh, 2000) to 10% (Rost et al., 2005), reaching up to 20% (Idehara, 2011) for some specific ULVZs. Furthermore, ULVZs have been inferred to occur as distinct patches, rather than as a globally ubiquitous layer (Idehara et al., 2007; Thorne & Garnero, 2004), and display large variability in lateral dimensions and seismic characteristics.

This broad range of observations makes it difficult to identify the plausible origin of ULVZs. Due to the large amplitude of the observed velocity reduction, which in some ULVZs is three times larger in shear wave

than in compression wave velocities, partial melting has often been suggested as a potential mechanism to explain these distinct regions (Andrault et al., 2012; Berryman, 2000; Hier-Majumder, 2008; Petitgirard et al., 2015; Revenaugh & Meyer, 1997; Williams & Garnero, 1996). However, some ULVZs display an equivalent reduction of both compressional and shear wave velocities that, together with the observed enhanced density by ~10% compared with the surrounding mantle, are difficult to explain by partial melting (Castle & Van Der Hilst, 2000; Hutko et al., 2009; Thorne & Garnero, 2004). Alternatively, a number of studies favor a solid state mechanism for the ULVZs and conclude that they represent a compositionally distinct, iron-enriched material that remains unidentified to date (Brown et al., 2015; Li et al., 2017; McNamara et al., 2010). Plausible candidates include for instance relicts of subducted slabs descending deep into the CMB region (Dobson & Brodholt, 2005; van der Hilst & Kárason, 1999), or products of fractional crystallization of a basal magma ocean trapped at the bottom of the mantle (Labrosse et al., 2007), such as iron-rich (Mg, Fe)SiO_3 perovskite (Nomura et al., 2011) or (Mg, Fe)O magnesiowustite (Wicks et al., 2010). Nevertheless, the most frequently proposed sources are core-mantle chemical reactions—either as a reaction between mantle silicates and outer core liquid iron alloy or as exsolution-solution processes—that result in the accumulation of Fe-enriched materials at the CMB (Dubrovinsky et al., 2004; Garnero & Jeanloz, 2000; Knittle & Jeanloz, 1991; Mao et al., 2006; Song & Ahrens, 1994). Iron-rich (Mg, Fe) O magnesiowustite (Bower et al., 2011; Wicks et al., 2010, 2017) and (Mg, Fe)SiO_3 post-perovskite (Mao et al., 2006) have received so far most attention as plausible candidates for the ULVZs based on their modal abundance and reasonable match between their sound velocities and the seismic observations (Mao et al., 2006; Wicks et al., 2010, 2017). In a recent study, FeO_2H_x—the potential product of a reaction between subducted hydrous minerals and core-iron (Liu et al., 2017)—has been proposed as a plausible candidate. Conversely, Knittle and Jeanloz (1991) experimentally investigated the interaction between (Mg, Fe)SiO_3 perovskite (Pv) and liquid iron at high *P-T* and showed the formation of stoichiometric FeSi at the D" region following the reaction:

$$(Mg_x,Fe_{1-x})SiO_3 + 3[(1-x)-s]Fe \rightarrow xMgSiO_3 + sSiO_2 + [3(1-x)-2s]FeO + [(1-x)-s]FeSi \quad (1)$$

Stoichiometric FeSi, which remains solid and adopts a B2-structure at CMB conditions (Fischer et al., 2013; Lord et al., 2010), may be an alternative Fe-rich candidate phase to explain the seismic anomalies at the bottom of the mantle. Yet, this phase has been largely omitted in compositional models of the CMB region due to the lack of constraints on their sound velocities and elasticity at relevant conditions. Current inferences on the elasticity of FeSi are based on extrapolations of ambient temperature V_P data on the low-pressure polymorph B20-FeSi (Badro et al., 2007) to core conditions through velocity-density systematics, that is, Birch's law, without temperature corrections. The recent identification of anharmonic effects on the compressional velocity-density relations on hcp-Fe (Lin et al., 2005; Sakamaki et al., 2016) and Fe-Si-alloys (Sakairi et al., 2018), however, stands against the application of Birch's law without further verification. Therefore, knowledge of the sound velocities and elasticity of B2-structured FeSi at relevant conditions is needed to assess the role of this phase as candidate material for the ULVZs.

Here we report investigations of the lattice dynamics of the high pressure B2-phase of FeSi at pressures up to 115(2) GPa and temperatures up to 1600(200) K by means of synchrotron based nuclear inelastic scattering (NIS) in laser-heated diamond anvil cells (LH-DACs). Our results, combined with available equations of state (Fischer et al., 2013; Sata et al., 2010), provide constraints on the evolution of the sound velocities of B2-FeSi at high pressure and temperature that serve as a test of validity for Birch's law and further demonstrate that this phase is a likely candidate to explain the ULVZs.

2. Experimental Methods

The ^{57}Fe-enriched B2-FeSi samples employed in this study were synthesized at 23 GPa and 1750 ± 50°C in a multi-anvil apparatus at BGI (Bayreuth, Germany). The synthesis was performed in a 10/4 cell assembly employing an Al_2O_3 capsule and a $LaCrO_3$ furnace with a heating duration of 90 min. The starting material was a stoichiometric mixture of Si and ^{57}Fe-enriched iron powders. The B2 structure and the stoichiometric proportion of the run products were confirmed by X-ray diffraction (XRD) and energy dispersive X-ray fluorescence spectroscopy (EDS), respectively.

The high-pressure high-temperature experiments were conducted in panoramic diamond anvil cells (DACs) specifically designed for NIS studies and depicted in Figure S1. The DACs were equipped with 120, 150, and 250 μm diamond culets depending on the target pressure. Beryllium gaskets were pre-indented down to 25–40 μm thickness, and a hole with a diameter of one third to half of the culet size was drilled in the gasket to serve as a sample chamber. Polycrystalline B2-FeSi samples with linear dimensions of $15 \times 15 \times 15$ μm^3 were loaded into the pressure chamber using KCl or Ne as both pressure transmitting medium and thermal insulator. The sample pressure was determined based on the phonon vibration of the T_{2g} mode of the diamond culet (Akahama & Kawamura, 2006). The pressure uncertainty was derived as standard deviation of the sample pressure measured before and after the NIS measurements. Samples were heated using a portable double-sided on-axis laser-heating (LH) system provided by the University of Potsdam (Spiekermann et al., 2020) with a nominal laser spot size of about 40 μm FWHM, that is, larger than the sample size. The design of the LH system is compatible with the collection geometry of NIS at 90° from the incident beam through the radial opening of the panoramic DAC. The surface temperatures of the samples were measured during the NIS experiments by spectroradiometry, whereas the bulk temperatures were refined afterward from the detailed balance of the NIS spectra (Chumakov & Rüffer, 1998).

NIS analyses were performed at the P01 high-resolution dynamics beamline of PETRA III, DESY (Wille et al., 2010). The storage ring was operated in timing mode with 40 bunches separated by 192 ns. The X-rays were monochromatized to 1.2 meV energy bandwidth using double channel cut Si(111) crystals, scanned around the ^{57}Fe nuclear resonance energy of 14.4 keV and focused down to 6.0×7.5 μm ($V \times H$) on the sample using Kirkpatrick-Baez mirrors. The incoherent inelastic scattering radiation emitted in a large solid angle was detected by counting the events between the incident X-ray pulses with two avalanche photo-diode detectors (APDs), which were inserted through the panoramic windows of the DAC and as close as possible to the sample. The energy dependence of the nuclear inelastic scattering was measured with steps of 0.2 meV in the energy ranges reported in Table S1. As the on-axis installation of the LH system prevents the positioning of an APD in the forward scattering direction, the energy profile of elastic nuclear scattering was measured at intervals between the laser-heated NIS scans. Typical collection times for each collected spectrum ranged between 8 to 15 h depending on the pressure-temperature conditions and the desired statistics. X-ray diffraction analysis of the quenched sample at 110(3) GPa after laser heating at 1600(200) K confirms the stability of the B2-FeSi crystal structure and the absence of chemical reaction between the sample and pressure medium and/or diamond (Figure S2).

We complemented the NIS study by room temperature Synchrotron Mossbauer Source (SMS) and Nuclear forward scattering (NFS) measurements in the B2-FeSi phase up to 48 and 113 GPa, respectively, including the same samples investigated by NIS here, to monitor the electronic state of sample and to rule out changes in the spin state that could affect the sound velocity data. Experimental details about the SMS and NFS data collection and the analysis are provided in the Supporting Information and in Figure S3.

3. Sound Velocities in FeSi at the Core-Mantle Boundary Region

NIS spectra of B2-FeSi were collected at 17 different pressures and temperatures from ambient conditions to 115(2) GPa and 1600(200) K (Figure 1). A quasi-harmonic approximation was applied to extract the partial phonon density of states (PDOS) associated with the resonant ^{57}Fe isotope from the collected NIS spectra (Figure S4) (Kohn & Chumakov, 2000; Sturhahn, 2000). The pressure and temperature evolution of the partial density of phonon states $g(E)$ of B2-FeSi is reported in Figures S5 and S6. The Debye sound velocity (V_D) was then obtained from the quantitative description of the low-energy region of the PDOS via

$$\lim_{E \to 0} \frac{g(E)}{E^2} = \frac{m_r}{2\pi^2 \hbar^3 \rho V_D^3} \tag{2}$$

where m_r is the molar mass of the resonant nucleus (in this case ^{57}Fe), $g(E)/E^2$ is the reduced partial density of phonon states (RDOS) and ρ is the density of the B2-FeSi sample (Chumakov et al., 2009; Hu et al., 2003). Selected NIS spectra and corresponding RDOS of B2-FeSi are shown in Figure 1. The contribution of the acoustic modes, that is, the Debye level, derived from a linear fit of the low energy range of the RDOS function (Figure 1b and Figure S7), is reported in Table S1, together with the calculated Debye sound velocities

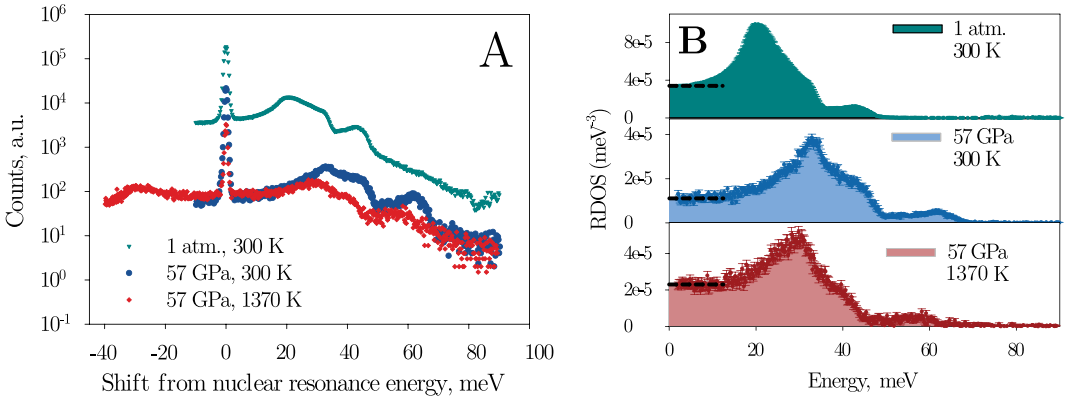

Figure 1. (a) Energy dependence of nuclear inelastic scattering (NIS) spectra of B2-FeSi at selected pressure and temperature conditions. The temperatures are determined from the NIS analysis. Energy zero refers to the nuclear resonance energy of ^{57}Fe. (b) Reduced partial density of phonon states ($g(E)/E^2$) of ^{57}Fe extracted from the spectra in (a). The dashed horizontal lines in (b) show the expected contribution of acoustic modes, that is, the Debye level, derived by linear fit of the low-energy region of the spectrum.

at each pressure-temperature conditions.In an isotropic media, the Debye sound velocity in materials with cubic symmetry is related to the aggregate compressional V_P and shear V_S wave velocities through the set of equations:

$$\frac{3}{V_D^3} = \frac{1}{V_P^3} + \frac{2}{V_S^3} \tag{3}$$

$$\frac{K_S}{\rho} = V_\phi^2 = V_P^2 - \frac{4}{3} V_S^2 \tag{4}$$

where V_ϕ is the bulk sound velocity, ρ is the density and K_S is the adiabatic bulk modulus. An approximate solution of Equations 3 and 4 derived by Sturhahn and Jackson (2007) and modified by Vasiukov et al. (2018) was further applied to calculate the aggregate velocities V_P and V_S as:

$$V_P = \sqrt{1.002\, V_\phi^2 - 0.104\, V_\phi V_D + 1.208\, V_D^2} \tag{5}$$

$$V_S = 0.952\, V_D - 0.041\, V_\phi \tag{6}$$

The adiabatic bulk modulus, K_S, is related to the isothermal bulk modulus K_T through the equation

$$K_S = K_T(1 + \gamma_{vib}\, \alpha\, T) \tag{7}$$

where γ_{vib} is the vibrational Grüneisen parameter, α is the thermal expansion coefficient and T is the temperature. Here the density ρ and the isothermal bulk modulus K_T of B2-FeSi were taken from an equation of state (EoS) derived by a joint fit of the *V-P-T* data sets from Fischer et al. (2013) and Sata et al. (2010) to a third-order Birch-Murnaghan EoS at 300 K and the Mie-Grüneisen parameterization at high-temperature. The derived thermal EoS parameters for B2-FeSi are presented in Table S3 and the calculated K_T reported in Table S2. The uncertainties of elastic parameters and densities of the B2-FeSi were determined from the full correlation matrix between the fit parameters as implemented in the EOS Fit program (Gonzalez-Platas et al., 2016). For the isothermal-adiabatic correction (Equation 7), the thermal expansion coefficient was derived from the thermal EoS (Table S3) and γ_{vib} was calculated via $\gamma_{vib} = \gamma_{vib,i}(V / V_i)^q$, where q is a fitting parameter and the subscript i refers to a reference phonon DOS. The phonon DOS scaling relation proposed by Murphy et al. (2011) was employed to describe the volume dependence of the B2-FeSi phonon DOS, and the B2-FeSi PDOS at ambient conditions was used as reference DOS for the calculations. The calculated bulk sound velocities V_ϕ and the aggregate velocities V_P and V_S are listed in Table S2. The errors for the V_D,

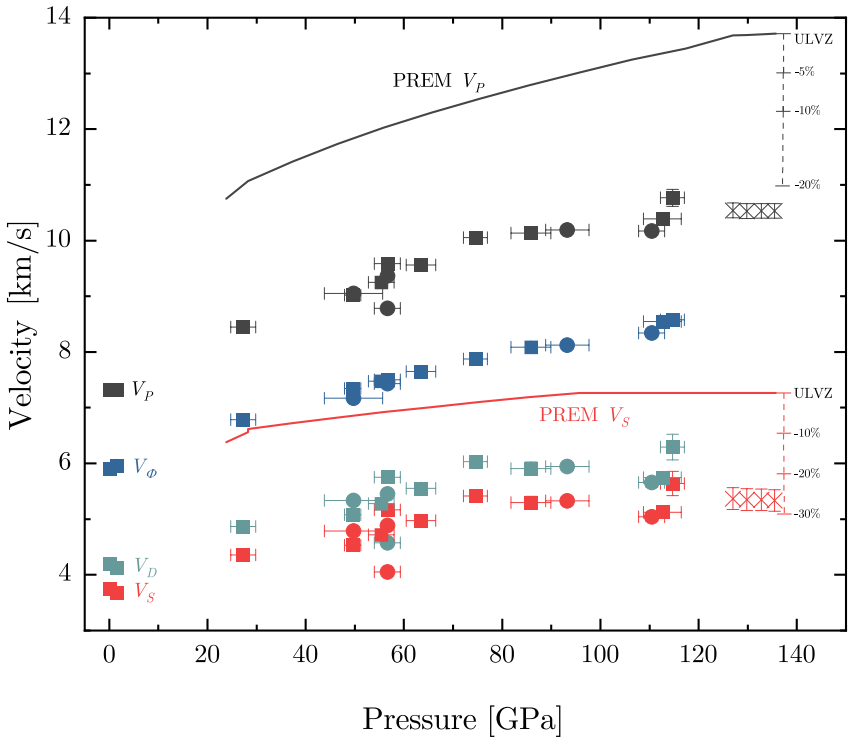

Figure 2. Velocities of B2-FeSi measured at high pressures and room temperature (rectangles), and at high pressures and temperatures (circles). Extrapolations of V_S and V_P of B2-FeSi to the *P-T* conditions of the D" layer are indicated by crosses. The V_S and V_P of the Preliminary Reference Earth Model (PREM) for lower mantle pressures and velocity decrements reported for ULVZs (see text for references) are shown for comparison.

V_P, and V_S were determined through error propagation of density, Debye level and elastic parameters uncertainties via Equations 2, 5 and 6 respectively. Figure 2 displays the pressure evolution of the Debye (V_D) and bulk (V_ϕ) sound velocities as well as the compressional (V_P) and shear (V_S) wave velocities for B2-FeSi at ambient and high temperature conditions derived from this study. All velocity sets increase monotonically with pressure and display little temperature dependence up to the highest temperature examined here, 1600 K. This observation contrasts with previous reports of strong anharmonicity of the compressional velocities of hcp-Fe (Lin et al., 2005; Sakamaki et al., 2016) and Fe-Si-alloys (Sakairi et al., 2018) at moderate pressures. To further assess the validity of the velocity-density systematics at high temperature, the Debye velocities of B2-FeSi at ambient and high temperature, which are the direct outcome of the present NIS study, are plotted against density in Figure 3. The linear dependence, regardless of the temperature, indicates that temperature affects V_D only insofar as it affects density. Hence, the application of Birch's law to extrapolate the Debye sound velocity of B2-FeSi to the conditions of the CMB region is validated. A least squares fitting of the combined room-*T* and high-*T* V_D-data by the Birch's law, $V = \alpha\rho + b$, including statistical weights, yields best-fit coefficients of $\alpha = 0.94 \pm 0.16$ and $b = -1.97 \pm 1.17$. The compressional (V_P) and shear (V_S) wave velocities at the conditions of the CMB region were calculated using Equations 3–7, employing the Debye sound velocities predicted by the Birch's law and thermoelastic parameters derived from the thermal EoS reported in Table S3. The results are displayed in Figure 2 and Figure S8.

4. Geophysical Implications

The shear wave velocities of B2-FeSi at the conditions of the D" are significantly lower compared to PREM and, within the errors, compare well with the lowest velocity limit (i.e., highest velocity reduction) observed for ULVZs (Figure 2). Moreover, we compare the sound velocities of B2-FeSi with those of other coexisting phases in lowermost mantle assemblages, that is, $MgSiO_3$, $CaSiO_3$ and $(Mg_{0.8}Fe_{0.2})O$, extrapolated to D" conditions using the thermodynamic formalism of Stixrude and Lithgow-Bertelloni (2005) and the ther-

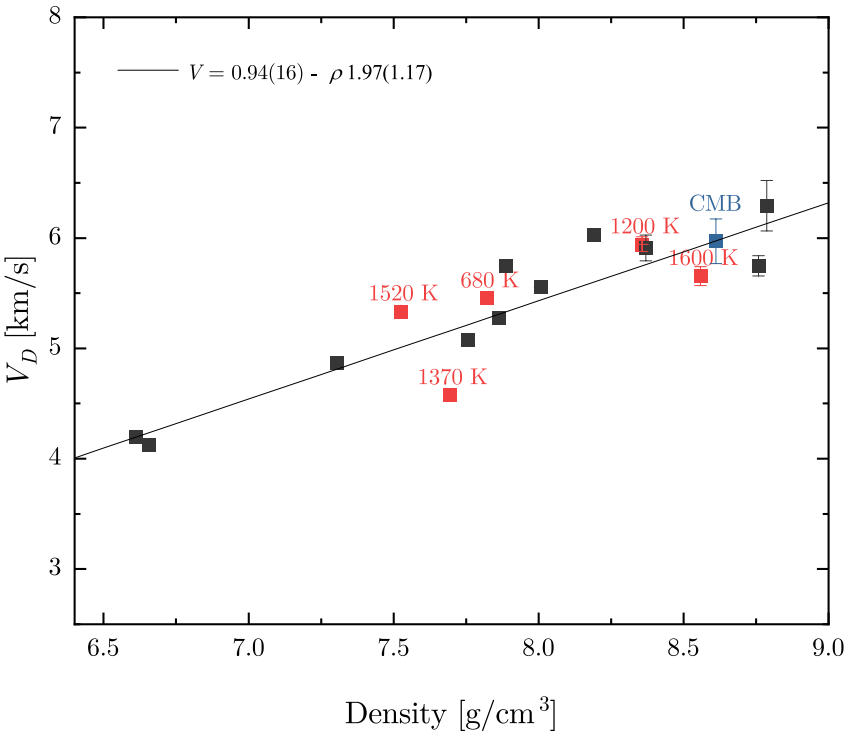

Figure 3. Debye sound velocities (V_D) of B2-FeSi as a function of density. Black rectangles, 300 K; red rectangles, at the indicated high temperatures. The line is a weighted least squares fit of the room and high temperature data by Birch's law, $V = \alpha\rho + b$ Values of B2-FeSi at the conditions of the core-mantle boundary, 136 GPa and 3950 K, are indicated for comparison.

moelastic data reported in Table S4. Our results indicate that B2-FeSi displays the lowest velocities among them (Figure S9), implying that FeSi-bearing lower mantle assemblages would have lower seismic velocities compared to an average mantle mineralogy.

To evaluate the effect of B2-FeSi on the seismic structure of the CMB region and to constrain the amount required to account for the ULVZ seismological observations, we further computed the sound velocity of a mantle assemblage resulting from chemical reactions between iron metal from the core and lower-mantle mineral phases as a function of the B2-FeSi content (Equation 1). For the calculations, the lower mantle assemblage was modeled assuming a pyrolitic bulk composition containing 75 vol% (Mg, Fe)SiO_3 bridgmanite, 18 vol% of (MgFe)O ferropericlase, and 7 vol% of $CaSiO_3$ Ca-perovskite (Irifune et al., 2010). It is important to notice that in such a core-mantle chemical reaction, the iron would not entirely be consumed to form FeSi, but rather incorporated in both FeSi and FeO as shown in Equation 1 (Knittle & Jeanloz, 1991). Further dissolution of FeSi in metallic iron is unlikely since the solubility of silicon in iron has been shown to decrease significantly to values below 1.5 wt.% at CMB conditions (Dubrovinsky et al., 2003; Fischer et al., 2013; Kuwayama et al., 2009; Ozawa et al., 2016). Moreover, it is assumed that FeO would form a solid solution with periclase. Considering these assumptions, the core-mantle chemical reaction leading to the formation of FeSi at the D" region would take the form:

$$\begin{aligned} CaSiO_3 + Mg_x\quad & Fe_{1-x}\,SiO_3 + (Mg_y\,Fe_{1-y})O + 3(1-x)Fe \\ & \rightarrow CaSiO_3 + (x\,MgSiO_3) + (1-x)FeSi + 3(1-x)FeO + Mg_y\,Fe_{1-y}O \end{aligned} \tag{8}$$

We have tested the effect of silica on the elastic properties of the aggregate produced by the reaction (Equation 1) (Figure S10). SiO_2 has only marginal effect on the aggregate velocities and only affects the density of the reaction assembly due to an increase of the initial Fe-content in (Mg, Fe)SiO_3 required for the reaction. Therefore we decided to exclude SiO_2 from the reaction (1) for simplicity. The presence of nickel alloying with iron in the reactive core melt has been neglected in the calculations because nickel will likely incor-

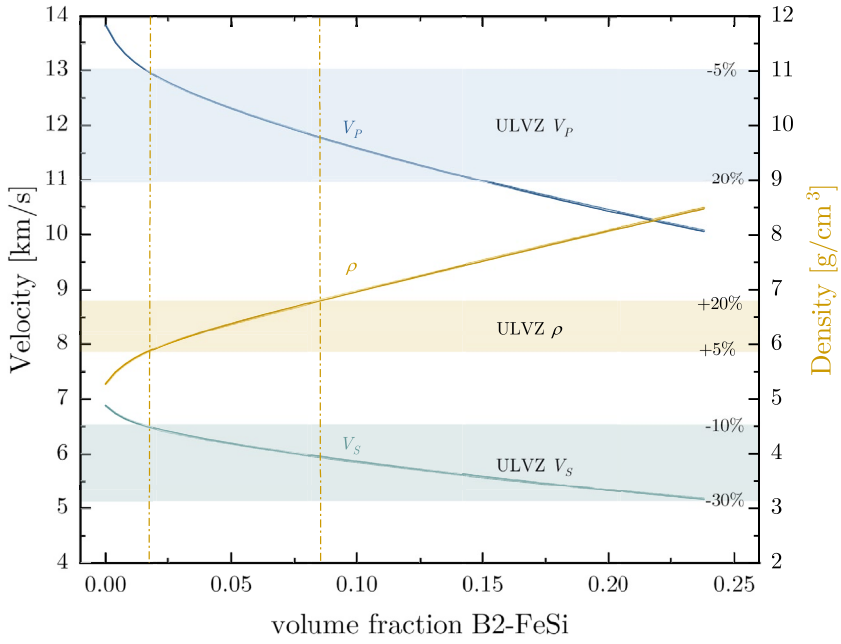

Figure 4. Aggregate density (ρ), and Voigt-Reuss-Hill average for compressional (V_P) and shear (V_S) wave velocities of a mixture of $MgSiO_3$, $CaSiO_3$, (MgFe)O, and B2-FeSi at 3950 K and 136 GPa presented as a function of the volume fraction of B2-FeSi in the aggregate (see Equation 8). Ranges of observed density and V_P and V_S decrements of ultralow-velocity zones (ULVZs) are shaded, respectively. The range of B2-FeSi proportion in the compound, for which both the aggregate velocities and density meet those of ULVZs, is indicated by the vertical dashed lines. The maximum volume fraction of B2-FeSi (0.24) in the mixture is limited by Equation 8.

porate in B2-FeSi as a FeSi-NiSi solid solution (Lord et al., 2014) and the effect of nickel alloying on sound velocities of Fe phases is very small (Lin et al., 2003). Reaction (Equation 8) thus provides a reasonable first approximation to chemical interactions at the bottom of the mantle. The exact molar fractions of the starting components were then derived from the pyrolitic model described above using a linearization fitting procedure. The maximum fraction of FeSi produced in the reaction is limited by the amount of (Mg, Fe)SiO_3-reactant to 0.24 (Figure 4). Note that x and y are not independent parameters, but are related by the partitioning coefficient for iron in the (Mg, Fe)SiO_3-(MgFe)O system. To account for iron partitioning between ferropericlase and bridgmanite, which is the stable structure of $MgSiO_3$ at D" conditions (Tateno et al., 2009), a partitioning coefficient of $K_D^{Pv/Mw} = 0.03$ was assumed based on the laser heating DAC data at the CMB conditions reported by Piet et al. (2016). As a consequence, ferropericlase is assumed to have an iron content significantly above 50%, even without considering the additional FeO fraction produced by the core-mantle reaction (Equation 8).

Subsequently, the aggregate velocities of a five-phase assemblage comprising $MgSiO_3$, $CaSiO_3$, FeO, MgO, and FeSi were computed from Voigt (upper bound) and Reuss (lower bound) averaging of the aggregate elastic moduli of each phase at CMB condition, 136 GPa and 3950 K (Dziewonski & Anderson, 1981; Hilst et al., 2007). For the calculations, the thermoelastic parameters of FeO in the high-spin state were employed as there is no evidence for the effect of spin-crossover on the sound velocities and elasticity of Fe-rich (MgFe)O even at room temperature (Wicks et al., 2017). As for B2-FeSi, the absence of discontinuity on the compression curve (Sata et al., 2010) and own SMS and NFS results that display a smooth decrease of the center shift (CS) upon compression allow ruling out any spin-transition that could affect the elastic properties in the pressure range of interest (Figure S3). Extrapolations were performed using the thermodynamic formalism described by Stixrude and Lithgow-Bertelloni (2005) and thermo-elastic parameters for each phase reported in Table S4. Densities were averaged using the Voigt bound. The aggregate sound velocities were then calculated from the averaged aggregate elastic moduli and density (Table S2) using Equations 9 and 10.

$$V_P = \sqrt{\frac{K_S + 4/3G}{\rho}} \quad (9)$$

$$V_S = \sqrt{\frac{G}{\rho}} \quad (10)$$

Figure 4 presents the aggregate density and Voigt-Reuss-Hill bound for both V_P and V_S of the core-mantle reaction assemblage as a function of the proportion of B2-FeSi. It can be seen that shear velocities of the aggregate model match those of the ULVZs for nearly the whole compositional range allowed by the reaction (Equation 8), that is, a range of a volume fraction of FeSi, whereas compressional wave velocities are solely matched for contents between 1.5 and 15.0 vol% B2-FeSi. These findings indicate that core-mantle chemical exchange leading to formation of a mineral aggregate containing moderate amounts of B2-FeSi could well be the source of ULVZs at the CMB. Although the core-mantle reaction would occur uniformly across the CMB, it could be limited by the maximum high of capillarity rise above the CMB, which is estimated to 20 m at most (Poirier et al., 1998). Viscous drag may thus be critical in explaining the heterogeneous spatial distribution of reaction products as it would contribute to concentrate the reaction products at region of mantle upwelling. The higher density of the Fe-rich phases would however prevent their entrainment into mantle plumes and would rather pile up at the bottom of the mantle forming the ULVZ (Dobson & Brodholt, 2005). This mechanism could account for the non-ubiquitous presence of ULVZs and the strong variability on their velocity reduction observed seismically (Thorne & Garnero, 2004; Idehara et al., 2007). Tighter constraints on the amount of B2-FeSi are provided by the computed density changes. To account for ULVZs, the assemblage issued from the core-mantle reaction must have a higher density than the ambient mantle at the respective depth for the constrained range of B2-FeSi proportion that matches ULVZ velocities. Figure 4 shows that the density of the model assemblage in the compositional range of 1.5–15.0 vol% B2-FeSi allowed by the aggregate velocities is larger compared to the density of the ambient mantle (~5.6 g/cm^3) and lower than the density of the outermost-core (~10 g/cm^3) immediately beneath the CMB. Moreover, the proportion can further be constrained by considering the density increase of 5%–20% observed in ULVZs compared to PREM. As inferred from Figure 4, the aggregate density matches that of ULVZs for an assemblage containing 1.8–8.4 vol% B2-FeSi. In conclusion, the findings herein indicate that even small amounts of B2-FeSi in a lower mantle assemblage would account for negative seismic velocity anomaly and enhanced density reported for ULVZ. Therefore, B2-structured FeSi has a fundamental role in explaining the origin of ULVZ and should be taken into account when modeling the structure and dynamics of the CMB region.

Acknowledgments
This research was partially supported by the German Research Foundation (DFG) through the DFG Project AOBJ:662965 GZ.:KU 3832/2-1 and start-up funds of WWU Münster. The authors acknowledge DESY (Hamburg, Germany), a member of the Helmholtz Association HGF, for the provision of beamtime. We thank Max Wilke (Universität Potsdam) for the provision of the laser heating system and the generous support of L. Libon and G. Spiekermann during the beamtime. V. Mergner gratefully acknowledges DESY and H.-C. Wille for providing an internship at beamline P01 of PETRA III, DESY. The authors acknowledge the European Synchrotron Radiation Facility for provision of synchrotron radiation facilities and we would like to thank A. I. Chumakov for assistance conduction SMS and NFS experiments and in using Nuclear Resonance beamline ID18. Open access funding enabled and organized by Projekt DEAL.

Data Availability Statement

The authors comply with AGU's data policy, and the NIS, X-ray diffraction, SMS and NFS data reported in this study are available in the repository https://uni-muenster.sciebo.de/s/vVeeVseoz3uV2v6.

References

Akahama, Y., & Kawamura, H. (2006). Pressure calibration of diamond anvil Raman gauge to 310 GPa. *Journal of Applied Physics*, *100*(4), 043516. https://doi.org/10.1063/1.2335683

Andrault, D., Petitgirard, S., Lo Nigro, G., Devidal, J.-L., Veronesi, G., Garbarino, G., & Mezouar, M. (2012). Solid-liquid iron partitioning in Earth's deep mantle. *Nature*, *487*(7407), 354–357. https://doi.org/10.1038/nature11294

Badro, J., Fiquet, G., Guyot, F., Gregoryanz, E., Occelli, F., Antonangeli, D., & D'Astuto, M. (2007). Effect of light elements on the sound velocities in solid iron: Implications for the composition of Earth's core. *Earth and Planetary Science Letters*, *254*(1–2), 233–238. https://doi.org/10.1016/j.epsl.2006.11.025

Berryman, J. G. (2000). Seismic velocity decrement ratios for regions of partial melt in the lower mantle. *Geophysical Research Letters*, *27*(3), 421–424. https://doi.org/10.1029/1999gl008402

Bower, D. J., Wicks, J. K., Gurnis, M., & Jackson, J. M. (2011). A geodynamic and mineral physics model of a solid-state ultralow-velocity zone. *Earth and Planetary Science Letters*, *303*(3), 193–202. https://doi.org/10.1016/j.epsl.2010.12.035

Brown, S. P., Thorne, M. S., Miyagi, L., & Rost, S. (2015). A compositional origin to ultralow-velocity zones. *Geophysical Research Letters*, *42*(4), 1039–1045. https://doi.org/10.1002/2014gl062097

Castle, J. C., & Van Der Hilst, R. D. (2000). The core-mantle boundary under the Gulf of Alaska: No ULVZ for shear waves. *Earth and Planetary Science Letters*, *176*(3–4), 311–321. https://doi.org/10.1016/S0012-821X(00)00027-3

Chumakov, A., Bosak, A., & Rüffer, R. (2009). Contribution of acoustic modes to the density of vibrational states measured by inelastic scattering techniques. *Physical Review B: Condensed Matter and Materials Physics*, *80*(9), 1–8. https://doi.org/10.1103/PhysRevB.80.094303

Chumakov, A., & Rüffer, R. (1998). Nuclear inelastic scattering. *Hyperfine Interactions*, *113*, 59–79. https://doi.org/10.1023/a:1012659229533

Dobson, D. P., & Brodholt, J. P. (2005). Subducted banded iron formations as a source of ultralow-velocity zones at the core–mantle boundary. *Nature*, *434*(7031), 371–374. https://doi.org/10.1038/nature03430

Dubrovinsky, L., Dubrovinskaia, N., Langenhorst, F., Dobson, D., Rubie, D., Geßmann, C., et al. (2003). Iron-silica interaction at extreme conditions and the electrically conducting layer at the base of Earth's mantle. *Nature*, *422*(6927), 58–61. https://doi.org/10.1038/nature01422

Dubrovinsky, L., Dubrovinskaia, N., Langenhorst, F., Dobson, D., Rubie, D., Geßmann, C., et al. (2004). Reaction of iron and silica at core-mantle boundary conditions. *Physics of the Earth and Planetary Interiors*, *146*(1–2), 243–247. https://doi.org/10.1016/j.pepi.2003.07.028

Dziewonski, A. M., & Anderson, D. L. (1981). Preliminary reference Earth model. *Physics of the Earth and Planetary Interiors*, *25*(4), 297–356. https://doi.org/10.1016/0031-9201(81)90046-7

Fischer, R. A., Campbell, A. J., Reaman, D. M., Miller, N. A., Heinz, D. L., Dera, P., & Prakapenka, V. B. (2013). Phase relations in the Fe-Fe-Si system at high pressures and temperatures. *Earth and Planetary Science Letters*, *373*, 54–64. https://doi.org/10.1016/j.epsl.2013.04.035

Garnero, E. J., & Helmberger, D. V. (1996). Seismic detection of a thin laterally varying boundary layer at the base of the mantle beneath the central-Pacific. *Geophysical Research Letters*, *23*(9), 977–980. https://doi.org/10.1029/95GL03603

Garnero, E. J., & Jeanloz, R. (2000). Fuzzy patches on the Earth's core-mantle boundary? *Geophysical Research Letters*, *27*(17), 2777–2780. https://doi.org/10.1029/2000GL008498

Gonzalez-Platas, J., Alvaro, M., Nestola, F., & Angel, R. (2016). EosFit7-GUI: A new graphical user interface for equation of state calculations, analyses and teaching. *Journal of Applied Crystallography*, *49*(4), 1377–1382. https://doi.org/10.1107/S1600576716008050

Hernlund, J. W., & McNamara, A. K. (2015). *The core-mantle boundary region* (Vol. 7, pp. 461–519). Elsevier B.V. https://doi.org/10.1016/B978-0-444-53802-4.00136-6

Hier-Majumder, S. (2008). Influence of contiguity on seismic velocities of partially molten aggregates. *Journal of Geophysical Research*, *113*(B12). https://doi.org/10.1029/2008jb005662

Hilst, R. D. V. D., Hoop, M. V. D., Wang, P., Tenorio, L., & America, B. C. (2007). Seismostratigraphy and thermal structure of Earth's core-mantle boundary region. *Science*, *315*, 1813–1818. https://doi.org/10.1126/science.1137867

Hu, M. Y., Sturhahn, W., Toellner, T. S., Mannheim, P. D., Brown, D. E., Zhao, J., & Alp, E. E. (2003). Measuring velocity of sound with nuclear resonant inelastic x-ray scattering. *Physical Review B: Condensed Matter and Materials Physics*, *67*(9), 094304.

Hutko, A. R., Lay, T., & Revenaugh, J. (2009). Localized double-array stacking analysis of PcP: D" and ULVZ structure beneath the Cocos plate, Mexico, central Pacific, and north Pacific. *Physics of the Earth and Planetary Interiors*, *173*(1–2), 60–74. https://doi.org/10.1016/j.pepi.2008.11.003

Idehara, K. (2011). Structural heterogeneity of an ultra-low-velocity zone beneath the Philippine Islands: Implications for core-mantle chemical interactions induced by massive partial melting at the bottom of the mantle. *Physics of the Earth and Planetary Interiors*, *184*(1), 80–90. https://doi.org/10.1016/j.pepi.2010.10.014

Idehara, K., Yamada, A., & Zhao, D. (2007). Seismological constraints on the ultralow velocity zones in the lowermost mantle from core-reflected waves. *Physics of the Earth and Planetary Interiors*, *165*(1), 25–46. https://doi.org/10.1016/j.pepi.2007.07.005

Irifune, T., Shinmei, T., McCammon, C. A., Miyajima, N., Rubie, D. C., & Frost, D. J. (2010). Iron partitioning and density changes of pyrolite in Earth's lower mantle. *Science*, *327*(5962), 193–195. https://doi.org/10.1126/science.1181443

Knittle, E., & Jeanloz, R. (1991). Earth's core-mantle boundary: Results of experiments at high pressures and temperatures. *Science*, *251*(5000), 1438–1443. https://doi.org/10.1126/science.251.5000.1438

Kohn, V. G., & Chumakov, A. I. (2000). DOS: Evaluation of phonon density of states from nuclear resonant inelastic absorption. *Hyperfine Interactions*, *125*(1), 205–221. https://doi.org/10.1023/A:1012689705503

Kuwayama, Y., Sawai, T., Hirose, K., Sata, N., & Ohishi, Y. (2009). Phase relations of iron-silicon alloys at high pressure and high temperature. *Physics and Chemistry of Minerals*, *36*(9), 511–518. https://doi.org/10.1007/s00269-009-0296-0

Labrosse, S., Hernlund, J. W., & Coltice, N. (2007). A crystallizing dense magma ocean at the base of the Earth's mantle. *Nature*, *450*(7171), 866–869. https://doi.org/10.1038/nature06355

Lay, T. (2015). 1.22—Deep Earth Structure: Lower Mantle and D". In G. Schubert (Ed.), *Treatise on geophysics* (2nd ed., pp. 683–723). Oxford: Elsevier. https://doi.org/10.1016/b978-0-444-53802-4.00019-1

Lay, T., Williams, Q., & Garnero, E. J. (1998). The core-mantle boundary layer and deep Earth dynamics. *Nature*, *392*(6675), 461–468. https://doi.org/10.1038/33083

Li, M., McNamara, A. K., Garnero, E. J., & Yu, S. (2017). Compositionally-distinct ultra-low velocity zones on Earth's core-mantle boundary. *Nature Communications*, *8*(1), 177. https://doi.org/10.1038/s41467-017-00219-x

Lin, J. F., Struzhkin, V. V., Sturhahn, W., Huang, E., Zhao, J., Hu, M. Y., & Hemley, R. J. (2003). Sound velocities of iron-nickel and iron-silicon alloys at high pressures. *Geophysical Research Letters*, *30*(21), 1–4. https://doi.org/10.1029/2003GL018405

Lin, J. F., Sturhahn, W., Zhao, J., Shen, G., Mao, H. K., & Hemley, R. J. (2005). Geophysics: Sound velocities of hot dense iron: Birch's Law revisited. *Science*, *308*(5730), 1892–1894. https://doi.org/10.1126/science.1111724

Liu, J., Hu, Q., Young Kim, D., Wu, Z., Wang, W., Xiao, Y., et al. (2017). Hydrogen-bearing iron peroxide and the origin of ultralow-velocity zones. *Nature*, *551*(7681), 494–497. https://doi.org/10.1038/nature24461

Lord, O. T., Walter, M. J., Dobson, D. P., Armstrong, L., Clark, S. M., & Kleppe, A. (2010). The FeSi phase diagram to 150 GPa. *Journal of Geophysical Research*, *115*(6), 1–9. https://doi.org/10.1029/2009JB006528

Lord, O. T., Wann, E. T. H., Hunt, S. A., Walker, A. M., Santangeli, J., Walter, M. J., et al. (2014). The NiSi melting curve to 70GPa. *Physics of the Earth and Planetary Interiors*, *233*, 13–23. https://doi.org/10.1016/j.pepi.2014.05.005

Mao, W. L., Mao, H.-k., Sturhahn, W., Zhao, J., Prakapenka, V. B., Meng, Y., & Hemley, R. J. (2006). Iron-rich post-perovskite and the origin of ultralow-velocity zones. *Science*, *312*(5773), 564–565. https://doi.org/10.1126/science.1123442

McNamara, A. K., Garnero, E. J., & Rost, S. (2010). Tracking deep mantle reservoirs with ultra-low velocity zones. *Earth and Planetary Science Letters*, *299*(1–2), 1–9. https://doi.org/10.1016/j.epsl.2010.07.042

Murphy, C. A., Jackson, J. M., Sturhahn, W., & Chen, B. (2011). Grüneisen parameter of hcp-Fe to 171 GPa. *Geophysical Research Letters*, *38*(24). https://doi.org/10.1029/2011GL049531

Nomura, R., Ozawa, H., Tateno, S., Hirose, K., Hernlund, J., Muto, S., et al. (2011). Spin crossover and iron-rich silicate melt in the Earth's deep mantle. *Nature*, *473*(7346), 199–202. https://doi.org/10.1038/nature09940

Ozawa, H., Hirose, K., Yonemitsu, K., & Ohishi, Y. (2016). High-pressure melting experiments on Fe-Si alloys and implications for silicon as a light element in the core. *Earth and Planetary Science Letters*, *456*, 47–54. https://doi.org/10.1016/j.epsl.2016.08.042

Petitgirard, S., Malfait, W. J., Sinmyo, R., Kupenko, I., Hennet, L., Harries, D., et al. (2015). Fate of $MgSiO_3$ melts at core-mantle boundary conditions. *Proceedings of the National Academy of Sciences*, *112*(46), 14186–14190. https://doi.org/10.1073/pnas.1512386112

Piet, H., Badro, J., Nabiei, F., Dennenwaldt, T., Shim, S.-H., Cantoni, M., et al. (2016). Spin and valence dependence of iron partitioning in Earth's deep mantle. *Proceedings of the National Academy of Sciences*, *113*(40), 11127–11130. https://doi.org/10.1073/pnas.1605290113

Poirier, J. P., Malavergne, V., & Le Mouël, J. L. (1998). *Is there a thin electrically conducting layer at the base of the mantle? In the core-mantle boundary region* (pp. 131–137). American Geophysical Union (AGU). https://doi.org/10.1029/gd028p0131

Reasoner, C., & Revenaugh, J. (2000). ScP constraints on ultralow-velocity zone density and gradient thickness beneath the Pacific. *Journal of Geophysical Research*, *105*(B12), 28173–28182. https://doi.org/10.1029/2000jb900331

Revenaugh, J., & Meyer, R. (1997). Seismic evidence of partial melt within a possibly ubiquitous low-velocity layer at the base of the mantle. *Science*, *277*(5326), 670–673. https://doi.org/10.1126/science.277.5326.670

Rost, S., Garnero, E. J., Williams, Q., & Manga, M. (2005). Seismological constraints on a possible plume root at the core-mantle boundary. *Nature*, *435*(7042), 666–669. https://doi.org/10.1038/nature03620

Sakairi, T., Sakamaki, T., Ohtani, E., Fukui, H., Kamada, S., Tsutsui, S., et al. (2018). Sound velocity measurements of hcp Fe-Si alloy at high pressure and high temperature by inelastic X-ray scattering. *American Mineralogist*, *103*(1), 85–90. https://doi.org/10.2138/am-2018-6072

Sakamaki, T., Ohtani, E., Fukui, H., Kamada, S., Takahashi, S., Sakairi, T., et al. (2016). Constraints on Earth's inner core composition inferred from measurements of the sound velocity of hcp-iron in extreme conditions. *Science Advances*, *2*(2), e1500802. https://doi.org/10.1126/sciadv.1500802

Sata, N., Hirose, K., Shen, G., Nakajima, Y., Ohishi, Y., & Hirao, N. (2010). Compression of FeSi, Fe_3C, $Fe_{0.95}O$, and FeS under the core pressures and implication for light element in the Earth's core. *Journal of Geophysical Research*, *115*(9), 1–13. https://doi.org/10.1029/2009JB006975

Song, X., & Ahrens, T. J. (1994). Pressure-temperature range of reactions between liquid iron in the outer core and mantle silicates. *Geophysical Research Letters*, *21*(2), 153–156. https://doi.org/10.1029/93gl03262

Spiekermann, G., Kupenko, I., Petitgirard, S., Harder, M., Nyrow, A., Weis, C., et al. (2020). A portable on-axis laser-heating system for near-90° X-ray spectroscopy: Application to ferropericlase and iron silicide. *Journal of Synchrotron Radiation*, *27*(2), 414–424. https://doi.org/10.1107/s1600577519017041

Stixrude, L., & Lithgow-Bertelloni, C. (2005). Thermodynamics of mantle minerals—I. Physical properties. *Geophysical Journal International*, *162*(2), 610–632. https://doi.org/10.1111/j.1365-246X.2005.02642.x

Sturhahn, W. (2000). CONUSS and PHOENIX: Evaluation of nuclear resonant scattering data. *Hyperfine Interactions*, *125*(1), 149–172. https://doi.org/10.1023/A:1012681503686

Tateno, S., Hirose, K., Sata, N., & Ohishi, Y. (2009). Determination of post-perovskite phase transition boundary up to 4400 K and implications for thermal structure in D" layer. *Earth and Planetary Science Letters*, *277*(1), 130–136. https://doi.org/10.1016/j.epsl.2008.10.004

Thorne, M. S., & Garnero, E. (2004). Inferences on ultralow-velocity zone structure from a global analysis of SPdKS waves. *Journal of Geophysical Research*, *109*(B8). https://doi.org/10.1029/2004JB003010

van der Hilst, R. D., & Kárason, H. (1999). Compositional heterogeneity in the bottom 1000 kilometers of Earth's mantle: Toward a hybrid convection model. *Science*, *283*(5409). https://doi.org/10.1126/science.283.5409.1885

Vasiukov, D. M., Ismailova, L., Kupenko, I., Cerantola, V., Sinmyo, R., Glazyrin, K., et al. (2018). Sound velocities of skiagite-iron-majorite solid solution to 56 GPa probed by nuclear inelastic scattering. *Physics and Chemistry of Minerals*, *45*(5), 397–404. https://doi.org/10.1007/s00269-017-0928-8

Wicks, J. K., Jackson, J. M., & Sturhahn, W. (2010). Very low sound velocities in iron-rich (Mg,Fe)O: Implications for the core-mantle boundary region. *Geophysical Research Letters*, *37*(15). https://doi.org/10.1029/2010gl043689

Wicks, J. K., Jackson, J. M., Sturhahn, W., & Zhang, D. (2017). Sound velocity and density of magnesiowüstites: Implications for ultralow-velocity zone topography. *Geophysical Research Letters*, *44*(5), 2148–2158. https://doi.org/10.1002/2016GL071225

Wille, H.-C., Franz, H., Röhlsberger, R., Caliebe, W. A., & Dill, F.-U. (2010). Nuclear resonant scattering at PETRA III: Brillant opportunities for nano—And extreme condition science. *Journal of Physics: Conference Series*, *217*, 12008. https://doi.org/10.1088/1742-6596/217/1/012008

Williams, Q., & Garnero, E. J. (1996). Seismic evidence for partial melt at the base of Earth's mantle. *Science*, *273*(5281), 1528–1530. https://doi.org/10.1126/science.273.5281.1528

References From the Supporting Information

Dewaele, A., Loubeyre, P., Occelli, F., Mezouar, M., Dorogokupets, P. I., & Torrent, M. (2006). Quasihydrostatic Equation of State of Iron above 2 Mbar. *Physical Review Letters*, *97*(21), 215504. https://doi.org/10.1103/PhysRevLett.97.215504

Fischer, R. A., Campbell, A. J., Shofner, G. A., Lord, O. T., Dera, P., & Prakapenka, V. B. (2011). Equation of state and phase diagram of FeO. *Earth and Planetary Science Letters*, *304*(3), 496–502. https://doi.org/10.1016/j.epsl.2011.02.025

Jacobsen, S. D., Reichmann, H.-J., Spetzler, H. A., Mackwell, S. J., Smyth, J. R., Angel, R. J., & McCammon, C. A. (2002). Structure and elasticity of single-crystal (Mg,Fe)O and a new method of generating shear waves for gigahertz ultrasonic interferometry. *Journal of Geophysical Research*, *107*(B2), ECV4-1–ECV4-14. https://doi.org/10.1029/2001jb000490

Kantor, I., Prakapenka, V., Kantor, A., Dera, P., Kurnosov, A., Sinogeikin, S., et al. (2012). BX90: A new diamond anvil cell design for X-ray diffraction and optical measurements. *Review of Scientific Instruments*, *83*(12), 125102. https://doi.org/10.1063/1.4768541

Katsura, T., Yoneda, A., Yamazaki, D., Yoshino, T., Ito, E., Suetsugu, D., & Jellinek, M. (2010). Adiabatic temperature profile in the mantle. *Physics of the Earth and Planetary Interiors*, *183*(1–2), 212–218. https://doi.org/10.1016/j.pepi.2010.07.001

Marquardt, H., Speziale, S., Reichmann, H. J., Frost, D. J., & Schilling, F. R. (2009). Single-crystal elasticity of $(Mg_{0.9}Fe_{0.1})O$ to 81 GPa. *Earth and Planetary Science Letters*, *287*(3–4), 345–352. https://doi.org/10.1016/j.epsl.2009.08.017

Murakami, M., Ohishi, Y., Hirao, N., & Hirose, K. (2012). A perovskitic lower mantle inferred from high-pressure, high-temperature sound velocity data. *Nature*, *485*(7396), 90–94. https://doi.org/10.1038/nature11004

Potapkin, V., Chumakov, A., Smirnov, G., Celse, J.-P., Rüffer, R., Mccammon, C., & Dubrovinsky, L. (2012). The Fe-57 synchrotron Mossbauer source at the ESRF. *Journal of Synchrotron Radiation*, *19*, 559–569. https://doi.org/10.1107/S0909049512015579

Prescher, C., Mccammon, C., & Dubrovinsky, L. (2012). MossA: A program for analyzing energy-domain Mössbauer spectra from conventional and synchrotron sources. *Journal of Applied Crystallography*, *45*, 329–331. https://doi.org/10.1107/S0021889812004979

Rüffer, R., & Chumakov, A. I. (1996). Nuclear resonance beamline at ESRF. *Hyperfine Interactions*, *97*(1), 589–604. https://doi.org/10.1007/BF02150199

Speziale, S., Zha, C.-S., Duffy, T. S., Hemley, R. J., & Mao, H.-k. (2001). Quasi-hydrostatic compression of magnesium oxide to 52 GPa: Implications for the pressure-volume-temperature equation of state. *Journal of Geophysical Research*, *106*(B1), 515–528. https://doi.org/10.1029/2000jb900318

Stixrude, L., & Lithgow-Bertelloni, C. (2011). Thermodynamics of mantle minerals—II. Phase equilibria. *Geophysical Journal International*, *184*(3), 1180–1213. https://doi.org/10.1111/j.1365-246X.2010.04890.x

Sturhahn, W. (2000). CONUSS and PHOENIX: Evaluation of nuclear resonant scattering data. *Hyperfine Interactions*, *125*(1–4), 149–172. https://doi.org/10.1023/A:1012681503686

Sturhahn, W., & Jackson, J. M. (2007). *Geophysical applications of nuclear resonant spec-troscopy* (Vol. 421, pp. 157–174). Geological Society of America. https://doi.org/10.1130/2007.2421(09)

Tange, Y., Takahashi, E., Nishihara, Y., Funakoshi, K.-i., & Sata, N. (2009). Phase relations in the system MgO-FeO-SiO_2 to 50 GPa and 2000°C: An application of experimental techniques using multianvil apparatus with sintered diamond anvils. *Journal of Geophysical Research*, *114*(B2). https://doi.org/10.1029/2008jb005891

Wolf, A. S., Jackson, J. M., Dera, P., & Prakapenka, V. B. (2015). The thermal equation of state of (Mg, Fe)SiO_3 bridgmanite (perovskite) and implications for lower mantle structures. *Journal of Geophysical Research: Solid Earth*, *120*(11), 7460–7489. https://doi.org/10.1002/2015jb012108

Xu, W., Lithgow-Bertelloni, C., Stixrude, L., & Ritsema, J. (2008). The effect of bulk composition and temperature on mantle seismic structure. *Earth and Planetary Science Letters*, *275*(1), 70–79. https://doi.org/10.1016/j.epsl.2008.08.012

Yang, R., & Wu, Z. (2014). Elastic properties of stishovite and the $CaCl_2$-type silica at the mantle temperature and pressure: An ab initio investigation. *Earth and Planetary Science Letters*, *404*, 14–21. https://doi.org/10.1016/j.epsl.2014.07.020

Zhang, Z., Stixrude, L., & Brodholt, J. (2013). Elastic properties of $MgSiO_3$-perovskite under lower mantle conditions and the composition of the deep Earth. *Earth and Planetary Science Letters*, *379*, 1–12. https://doi.org/10.1016/j.epsl.2013.07.034